10582 *Biochemistry* **2009,** *48,* 10582–10590
DOI: 10.1021/bi900960s

BIOCHEMISTRY
including biophysical chemistry & molecular biology
Article

Influence of Aggregation Propensity and Stability on Amyloid Fibril Formation As Studied by Fourier Transform Infrared Spectroscopy and Two-Dimensional COS Analysis[†]

Núria Cerdà-Costa,[‡,∥] Igor De la Arada,[§,∥] Francesc X. Avilés,[‡] José L. R. Arrondo,[§] and Sandra Villegas*[,‡]

[‡]*Departament de Bioquímica i Biologia Molecular and Institut de Biotecnologia i Biomedicina, Universitat Autònoma de Barcelona, 08193 Cerdanyola del Vallès, Spain, and* [§]*Unidad de Biofísica (centro mixto CSIC-UPV/EHU) and Departamento de Bioquímica y Biología Molecular, Universidad del País Vasco, Bilbao, Spain* [∥] *These authors contributed equally to this work.*

Received June 8, 2009; Revised Manuscript Received October 2, 2009

ABSTRACT: Understanding the process of amyloidogenesis is important for the future treatment of misfolding-based diseases, such as Alzheimer's, spongiform encephalopathies, and other important disorders affecting humans. In this work, we have used one of the best-characterized models for folding and misfolding, the activation domain of human procarboxypeptidase A2 (ADA2h). The wild type (WT) and three mutants affecting the kinetics of aggregation have been studied by IR from the folded state at acidic pD to fibril formation, showing the disappearance of structured features prior to a dramatic increase in the magnitude of the amyloid-characteristic band upon temperature induction. Transmission electron microscopy (TEM) shows that amyloid fibrils are formed under the conditions used in this work. The kinetics of the process observed for WT is clearly affected by the aggregation tendency and the stability of each mutant, although the final state is the same. Our conclusion is that this domain is nucleated prior to the conformational reorganization rendering the final amyloid fibril, which is ultimately reached in a manner independent of the aggregation tendency and the stability of each variant.

The process that a polypeptide chain undergoes to form amyloid fibrils is of critical interest because of its involvement in the conformational diseases termed amyloidoses. The occurrence of these highly ordered aggregates has been observed not only in disease-related proteins but also in apparently nonpathogenic species, suggesting that they could represent a conformational state in all polypeptide chains (*1*). Recent investigations have led to the hypothesis that protein aggregation is in direct competition with protein folding, describing a double funnel for the conformational landscape (*2*), where different sequence stretches are governing each process (*3*). In short, intramolecular contacts among residues would lead to the formation of the native structure, whereas intermolecular contacts would produce an aggregated structure, being ordered (amyloid fibrils) or not (amorphous aggregates) (*2*).

Several studies have been centered on the modulation of amyloid fibril propensity because of the polypeptide sequence (*4*, *5*) leading to the creation of a predictive formula or programs that can shed some light on the putative consequences of mutations in proteins (*4*, *6*, *7*). Besides aggregation propensity, understanding structure conversion produced in the amyloid formation process is also necessary to complete the understanding of the entire picture. Eisenberg et al. (*8*) proposed three general models accounting for monomer structural reorganization in fibril formation. Whereas two of the conversion models (the refolding and the natively disordered models) involve the reorganization of the entire polypeptide chain, the gain-of-interaction model proposes that only a small conformational change takes place, with exposure of a previously hidden surface that will interact with equivalent surfaces of other monomers.

Infrared spectroscopy (IR)[1] has been extensively used to follow amyloid formation. Coupled with two-dimensional correlation analysis (2D-COS) (*9*, *10*), it allows for a more detailed analysis of the secondary structure conversion from the initial monomer to the amyloid fibril. In this approach, the different spectra obtained upon application of an external perturbation are correlated to increase resolution and to gain better insight into the relationship between bands (*11*−*13*).

In this work, one- and two-dimensional infrared correlational spectroscopy has been applied to the study of the formation of amyloid fibrils from the native state of the activation domain of human procarboxypeptidase A2 (ADA2h) and three mutants with different aggregation propensities, using temperature as the perturbing agent. ADA2h has been used as a model protein for amyloid-like fibril formation at acidic pH (*14*, *15*), since a thorough understanding of its folding mechanism at neutral pH has already been demonstrated (*16*−*22*). Moreover, the creation of a large battery of single-residue variants has provided detailed information about the amyloid forming propensity changes upon mutation and the relevance of sequence context and residual structure in the overall process (*5*). The most

[†]S.V. has financial funding from Grant PI07-0148 and the Fundación Mutua Madrileña (FMM-2008). N.C.-C. is supported by a DURSI (Generalitat de Catalunya) fellowship (2003 FI 00388). J.L.R.A. is the recipient of Grant BFU2006-14423 from MEC.

*To whom correspondence should be addressed: Dpt. Bioquímica i Biologia Molecular, Unitat de Biociències, UAB, Campus Bellaterra, 08193 Spain. Telephone: 34 93 581 4258. Fax: 34 93 581 1264. E-mail: sandra.villegas@uab.cat.

[1]Abbreviations: ADA2h, activation domain of human procarboxypeptidase A2; WT, wild-type; TEM, transmission electron microscopy; FT-IR, Fourier transform infrared spectroscopy; 2D-COS, two-dimensional correlation analysis; CD, circular dichroism; UV, ultraviolet.

 Published on Web 10/12/2009

noticeable finding was a conformational reorganization of the aggregation nucleus in the very early kinetics of amyloid fibril formation by ADA2h from the denatured state.

The temperature-induced aggregation kinetics from the native state at acidic pD for the wild-type (WT) variant, a slowly aggregating mutant (I23V), a rapidly aggregating mutant (N58A), and a nonprone-to-aggregation mutant (F65A) (*5*) followed by IR allows us to compare the conformational changes of the different processes upon mutation. TEM and CD characterization reinforce the obtained results.

MATERIALS AND METHODS

Materials. ADA2h variants were expressed in a BL21(DE3) *Escherichia coli* strain using a modified pTZ18U vector (*19*). Oligonucleotides were synthesized by Roche Molecular Biochemicals. Slide-A-Lyzer 3500 MWCO Mini Dialysis Units were purchased from Pierce. All other reagents were obtained from Sigma-Aldrich.

Expression and Purification. Expression and purification of all variants were conducted as previously described (*5*), and the obtained proteins were concentrated and adjusted to 5 mg/mL (544 μM) in 50 mM sodium phosphate (pH 7). The variants are ~9.2 kDa and pI ~4.4. Sequence information can be obtained from ref *5*.

Infrared Analysis. The four variants were dialyzed overnight against 25 mM glycine (pD 3.0) at 4 °C, using Slide-A-Lyzer 3500 MWCO mini Dialysis Units and D_2O as a solvent. The completeness of H → D exchange was monitored by the disappearance of the amide II band (1545 cm^{-1}). A sample of the WT protein in 50 mM sodium phosphate (pD 7.0) was also analyzed.

The spectra were recorded in a Nicolet 5700 spectrometer (Thermo, Madison, WI) using a Peltier mount and excavated cells with a 50 μm path (Biotools, Wacounda, IL). The spectra were acquired using the Series software licensed under OMNIC (Thermo). The sample at pD 3 was heated from 20 to 90 °C in 10 min and maintained afterward at 90 °C for 30 min. Typically, 305 spectra were averaged for each minute. The series obtained was ratioed against a background, producing the absorbance spectra with a nominal resolution of 2 cm^{-1}. Data treatment and band decomposition of the original amide have been described previously (*23*). In short, the number and position of the component bands are obtained by deconvolution and derivation. Bandwidths are estimated from the derivatives. The bandshape is set to 90% of a Gaussian curve. The fitting is obtained by iteration in two steps: band positions are fixed in a first iteration and free in the second. The mathematical solution to the decomposition may not be unique, but if restrictions are imposed, such as the maintenance of the initial band positions at an interval of ± 1 cm^{-1} and bandwidth preservation within the expected limits of the agreement with theoretical boundaries or predictions, the result becomes, in practice, unique.

To obtain the 2D-COS infrared maps, we used an incubation time at 90 °C as the perturbation to induce spectral fluctuations and to detect dynamic spectral variations of the secondary structure of the four variants. The two-dimensional synchronous and asynchronous spectra have been obtained previously with other protein models (*24*). Correlations between bands are found through the so-called synchronous and asynchronous spectra that, respectively, correspond to the real and imaginary parts of the cross correlation of spectral intensities at two wavenumbers. In a synchronous 2D map, the peaks located in the diagonal (autopeaks) correspond to changes in intensity induced by the external perturbation and are always positive. When a cross-correlation peak is positive, it indicates that both bands involved undergo either an increase or a decrease; on the other hand, a negative cross-correlation peak reflects the fact that one of the two bands is increasing in intensity while the other is decreasing.

Transmission Electron Microscopy. One hundred microliters of each variant was dialyzed overnight against 25 mM glycine (pD 3) and heated in the same manner as in the infrared experiments to trigger the aggregation process. Samples were taken before heating and 30 min and 2 days after induction of fibrillation. The samples were then diluted 1/20 in Milli-Q water and quickly adsorbed to glow-discharged carbon-coated grids. The material was stained using the method described elsewhere (*25*) and also used previously with ADA2h (*5*).

The samples were visualized with a Hitachi H-7000 microscope in the Servei de Microscòpia of Universitat Autònoma de Barcelona.

Circular Dichroism. The protein variants were diluted to 200 and 20 μM with 50 mM phosphate buffer (pH 7) for the native CD measurements. The same variants were also taken to 2 mg/mL and dialyzed overnight against 25 mM glycine (pH 3) at 4 °C. The dialyzed samples were then taken to 200 and 20 μM with the dialysis buffer, heated at 95 °C for 5 min, to properly activate protein aggregation, and left overnight at room temperature. Cuvettes with path lengths of 0.2 and 0.02 cm were used for the circular dichroism measurements with 20 and 200 μM samples, respectively, and 20 scans recorded at 100 nm min^{-1} (response of 1 s) in a JASCO 715 spectrophotopolarimeter were averaged for each variant.

To calculate the relative contribution of each secondary structure, we deconvolved spectra with the CDSSTR analysis program from the DICHROWEB server (*26*, *27*) using the SP175 reference set (*28*).

RESULTS

Assignment of Initial Infrared Bands in the Wild-Type Protein. The structure and fibril formation process of the activation domain of human procarboxypeptidase A2 (ADA2h) have been studied by infrared spectroscopy via examination of the changes produced in the amide I′ band region located between 1700 and 1600 cm^{-1} and arising mainly from the C=O stretching vibration of the peptide bond. Figure 1A shows the deconvolved spectra at the most relevant times during fibril formation, and Figure 2 shows the band decomposition of the infrared spectra (see also Figure 1 of the Supporting Information). It can be seen that there are two major bands whose intensities increase, located at ~1682 and ~1619 cm^{-1}, and the variations in other bands when the spectra corresponding to the process are compared. The most important change in ADA2h at acidic pD (*14*) is the appearance of a prominent band at ~1619 cm^{-1}, which has also been described in other fibril formation processes (*29*, *30*) and was previously reported to be missed at pD 7 (*14*). The band decomposition of the IR spectrum at neutral pD obtained in this work is shown in Figure 2 for the sake of comparison.

Before the induction of fibril formation (Figure 2, 0 min), the spectrum shows seven bands at 1682, 1671, 1660, 1647, 1632, 1619, and 1606 cm^{-1}, the latter corresponding to amino acid side chains. ADA2h is an α/β-protein, according to structural studies (*31*, *32*). Therefore, the other bands of the spectrum would correspond to ADA2h initial secondary structure components: α-helices (1647 cm^{-1}, partially unfolded with respect to that at

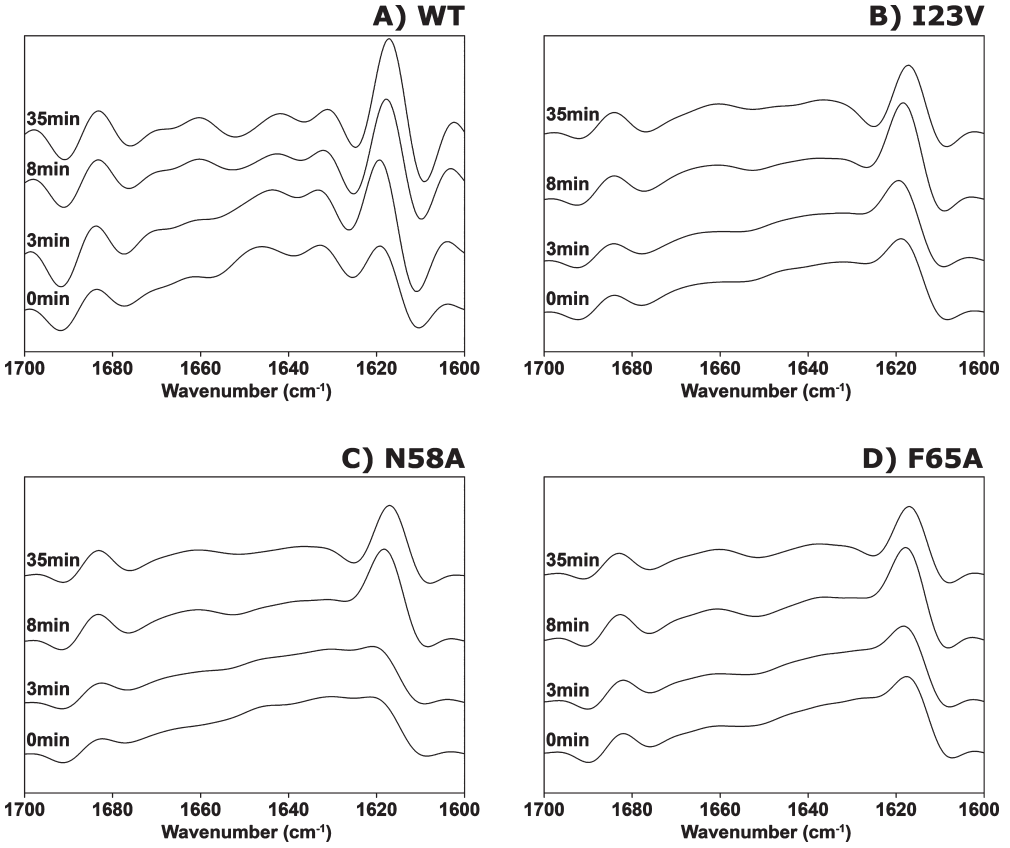

FIGURE 1: Time course of the formation of amyloid fibrils by four variants of ADA2h followed by FT-IR. The spectra at the most significant times are represented in this figure, from bottom to top: 0, 3, 8, and 35 min. In all cases, the formation of a band positioned at 1619 cm^{-1} must be noted, coupled with a slight increase in the magnitude of the 1682 cm^{-1} band.

neutral pD located at 1652 cm^{-1}), native antiparallel β-sheet (1682 and 1632 cm^{-1}), and elements of irregular secondary structure (1671 and 1660 cm^{-1}). The percentage of each amide component is shown in Tables 1 and 2 of the Supporting Information.

Formation of Amyloid Fibrils by the Wild-Type Protein. As seen in Figures 1 and 2, during heat induction, the number of bands does not change but their position and percentage area are different, producing a changed amide I′ band shape. The 1619 cm^{-1} band is already present in the acidic pD sample, as opposed to the neutral-pD protein. This is indicative of a certain aggregation at initial times, which might be quite different from that by amyloid fibrils (although also rich in extended structure) since the transmission electron micrograph at time zero does not show the typical amyloid architecture (Figure 4). Afterward, the 1619 cm^{-1} band experiences a dramatic increase in area, especially after 8 min (see Table 1 and Figure 2 of the Supporting Information), coupled with a shift of its position to lower wavelengths, corresponding to a conformational reorganization that leads to the amyloid fibril. The reorganization of the initial nucleus of the fibril formed by ADA2h has previously been reported by following the early kinetics of the process from the unfolded state using a stopped-flow method coupled to circular dichroism (CD) (*5*). The above-mentioned shift (from 1619 to 1616 cm^{-1}) indicates a stronger interaction within the reorganized and late fibril. The other bands show shifts and decreases in area indicative of an unfolding process simultaneous with the nucleation and growth of the fibril.

Effect of Mutations in Fibril Formation. Several mutants of ADA2h were previously constructed to destabilize its fold (*19*), while others have been recently designed to change the kinetics of amyloid fibril formation (*5*). The early kinetics of aggregation of all of them has recently been reported (*5*). For this work, we have chosen a rapid one, N58A, a slower one, I23V, and one not prone to aggregation, F65A. It is important to note that when aggregation is being studied concentration is a key factor. In our previous work, a protein concentration of 40 μM was used instead of the concentration of 544 μM presented in this study, and we pointed out that even the variant least prone to aggregation shall aggregate with an increase in concentration (*5*). The increase of more than 10-fold in this work is a consequence of the different techniques used in both studies (CD coupled with stopped-flow and IR).

The ability to form fibrils by these variants has been studied using the same conditions that were used for the native protein. The amide I′ band has been analyzed during the fibrillation process (Figure 1). Quantification of decomposed bands at the relevant times for the wild-type protein and its variants is presented in the Supporting Information (Tables 1 and 2). The main conclusion is that, whereas during the nucleation phase the processes are not equivalent for the different mutants, the final spectra are similar, indicating that mutations affect the propensity of the protein to aggregate, but not the fibril structure.

The initial area of the band at 1619 cm^{-1} of each variant (18.6% for I23V, 18.6% for F65A, and 20.3% for N58A) is higher than that of the WT (14.3%) (Table 1 and Figure 2 of the Supporting Information), as expected for destabilizing mutations. Nevertheless, this effect is especially evident for variant N58A, the one most prone to aggregation. With regard to the final area of this band, a similar percentage is shown by all of the

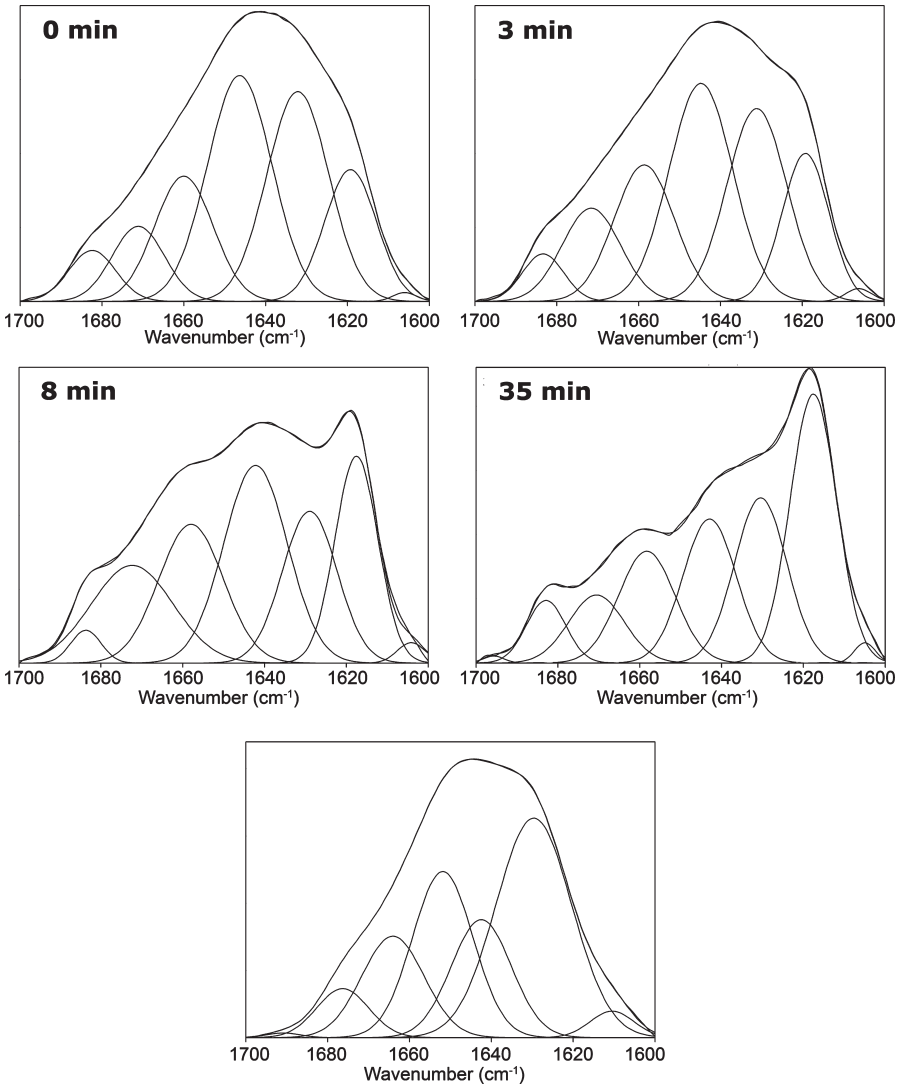

FIGURE 2: Band decomposition of the amide I′ spectra of amyloid formation kinetics for WT ADA2h. Band decomposition at the most relevant times of the aggregation kinetics (0, 3, 8, and 35 min) of the WT variant of ADA2h at acidic pD. The bottom panel shows band decomposition for WT ADA2h at pD 7 (native soluble form) lacking the 1619 cm^{-1} band.

mutants at the end of the process. These results would indicate that mutations produce conformational changes during the aggregation pathway; however, since the environment's influence remains the same, they do not alter the pattern of the final fibril.

Two-Dimensional Correlation Spectra. To reveal interaction between bands for the changes occurring during the process of fibril formation, 2D-COS spectra have been plotted (Figure 3). In the synchronous map, the autopeaks (diagonal) reflect intensity and are always positive. The cross-correlation peaks indicate a relationship between the two bands involved (*9*−*13*, *24*). Two clear autopeaks are present in the diagonal of the map of the wild-type protein (Figure 3A). One predominant band, located at 1616 cm^{-1}, indicative of the amyloid fibril and the other centered around 1647 cm^{-1} associated with partially unfolded α-helices are present. When the 1616 cm^{-1}−1647 cm^{-1} cross-correlation peak is considered, a negative correlation is found between them, thus pointing out that the growth of the amyloid fibril is mainly due to the disappearance of this secondary structure. Even if no autopeak is seen at 1682 cm^{-1}, the other component of the amyloid fibril (and also the minor component of the native antiparallel β-sheet), the presence of the 1682 cm^{-1}−1647 cm^{-1} less intense cross-correlation peak indicates that the change in the intensity of this band, although smaller, is actually detected. No intensities seem to be associated with the low-frequency, and main, β-sheet component. However, the above-mentioned main cross-correlation peak (1616 cm^{-1}−1647 cm^{-1}) is quite broad, ranging from native β-sheets (1632 cm^{-1}) to β-turns (1675 cm^{-1}), thus reflecting the stated observation that β-sheets of some native proteins are different from those in amyloid fibrils and that a substantial reorganization is necessary to form the fibril (*30*, *33*).

The synchronous maps of the mutants resemble that for the wild-type protein (Figure 3B−D), although their cross-correlation peaks appear broader when compared to it. This reflects the broadening of almost all bands present in their spectra (see Figure 1) and is a consequence of their lower conformational stability. The fact that the mutants show a strong autopeak around 1625 cm^{-1}, not present in the wild-type map, is noteworthy. This autopeak is a reflection of the minimum preceding the aggregated β-sheet band at 1616 cm^{-1}, the magnitude of which strongly decreases in each of them (see also Figure 1). This can be especially observed in I23V, where the magnitude of the 1616 cm^{-1} band does not increase very much, and therefore, a

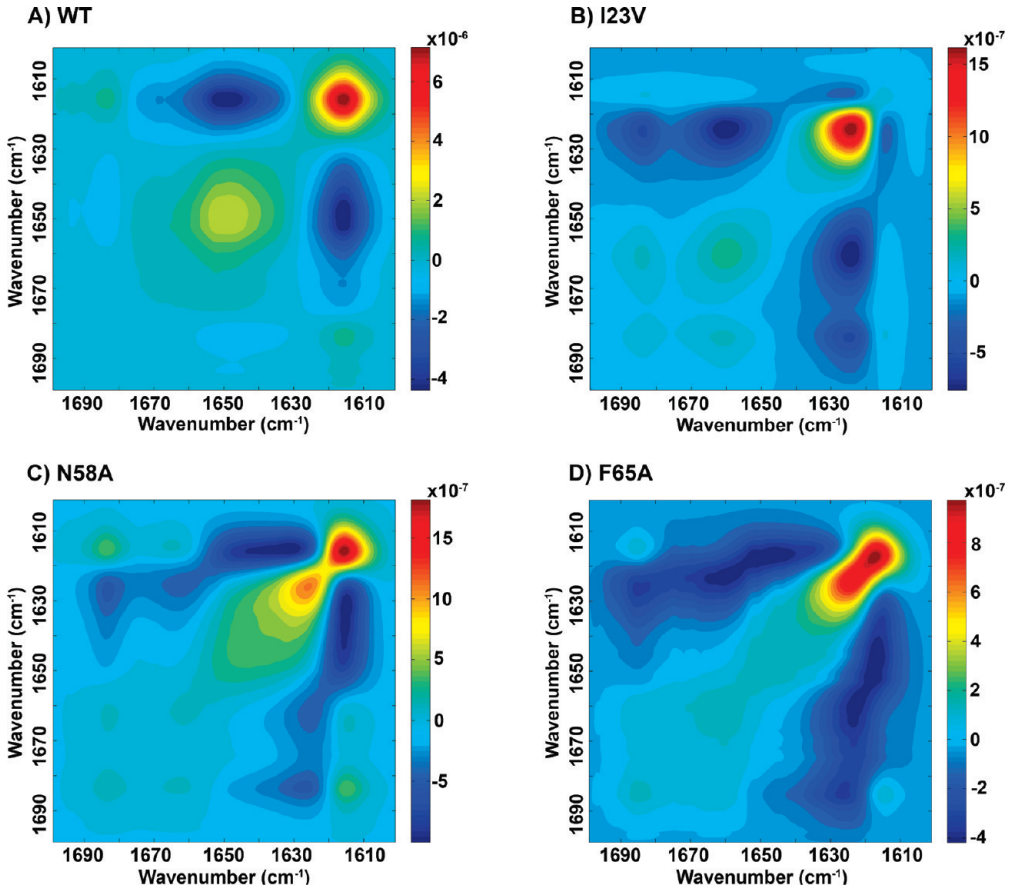

FIGURE 3: Synchronous maps of the FT-IR spectra for aggregation kinetics. The synchronous maps for all mutants are represented using the two-dimensional correlation analysis applied to the FT-IR spectra: (A) WT, (B) I23V, (C) N58A, and (D) F65A. The positive correlations are shown in different shades of red according to their intensities and the negative ones in blue.

corresponding autopeak cannot be found. Moreover, all mutants exhibit an autopeak at 1682 cm^{-1}, albeit rather faint, which is a reflection of the increase in the magnitude of this band during amyloid fibril formation.

Electron Microscopy. Electron micrographs demonstrate that the process leads to formation of amyloid fibrils and not just to an amorphous protein aggregate (Figure 4). In contrast to the nucleated dependent kinetics leading to amyloid fibrils (*34*), N58A, F65A, and WT ADA2h show, at time zero, some worm-like fibrils like those described by Radford and colleagues for the assembly of spherical or prefibrillar material of β_2-microglobulin that follow a non-nucleated dependent kinetics (*33*−*35*). Nevertheless, no such wormlike structures were unequivocally observed for I23 V (see Discussion). In this work, this wormlike state has been depopulated by temperature, which allows for the initiation of the fibril formation process. The fact that this process is different for each variant, as confirmed by the synchronous maps (Figure 3), indicates that these wormlike structures would be conformationally different. The wormlike structures observed for the variants, with the exception of I23V, are approximately 80−100 nm long and 8−9 nm wide. It is noteworthy that F65A wormlike fibrils seem to be more organized than the ones obtained for the other variants (see Discussion).

At 30 min (time required to prepare the TEM samples), after the samples have been heated in the same way as in the IR experiments, all of the variants show organized fibrillar material. At longer periods, the fibrils are very similar and better defined in all the variants, indicating that the structure attained is similar for all protein samples studied.

Circular Dichroism. Figure 5 shows the far-UV CD spectra of the variants at neutral and acidic pH measured at two different concentrations, 20 and 200 μM. At pH 7, there is no aggregation and the spectra obtained at 200 μM are identical to those at 20 μM (results not shown). It is important to note that the samples at pH 3 were induced to form amyloid fibrils when heated at 95 °C for 5 min and, as a consequence, do not correspond to the conditions of the IR experiment at time zero. In any case, the concentration used for IR, 544 μM, is too high to be studied by CD, especially in the very far UV region (210−190 nm) where the detector is saturated and no reliable information can be obtained. Thus, the CD data presented here must be regarded as information complementary to the structural analyses derived from the IR final spectra.

The $\alpha + \beta$ structure of the wild type is maintained for all three mutants at neutral pH. The deconvolved CD spectra (Table 1) show an α-helix content of 31−32% for all of them, with the exception of F65A, the level of which slightly decreases to 27%, favoring an equivalent increase in β-sheet content. This difference is due to the instability of mutant F65A. It is important to note that the F65 side chain interacts with the V64 backbone, one of the main components of the hydrophobic core (*19*).

At acidic pH and upon temperature induction, the WT variant shows a loss in helical content enhancing the weight of the β-sheet conformation, as previously described (*14*). This feature agrees with the differential location of the IR band for α-helices at acidic and neutral pD [1647 and 1652 cm^{-1}, respectively (Figure 2)]. At 20 μM, 8% of the helical content is lost in favor of an increase in

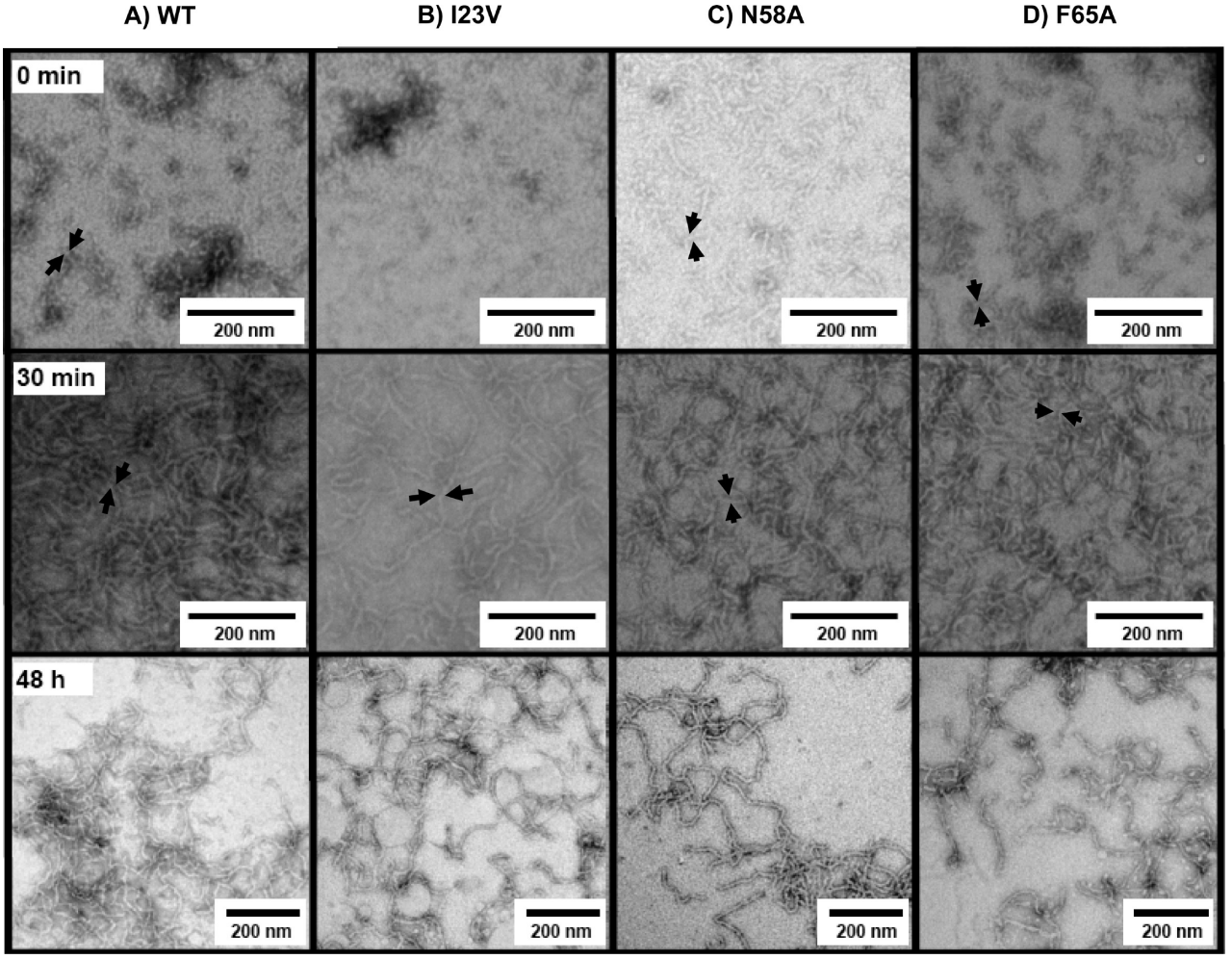

FIGURE 4: Transmission electron micrographs at discrete points of the amyloid fibril formation process by WT ADA2h (A) and mutants I23V (B), N58A (C), and F65A (D). The micrographs at time zero show the presence of weakly structured aggregates, and the formation of a huge amount of amyloid fibrils completely covering the grid can be seen as little as 30 min after induction for all variants. These amyloid fibrils, however, are far more structured after 48 h.

β-sheet content, whereas the levels of β-turns and random coils remain the same. However, at 200 μM there is a dramatic loss of 24% of the helical content in favor of an increase in β-sheet content (18%) and also random coil content (6%). The effect of acidic pH is more remarkable for mutants I23V and N58A than for the WT, but especially for N58A, the most prone to amyloid fibril formation. N58A shows very similar spectra at both concentrations, reaching high β-sheet content at the lower concentration. Moreover, as was the case for the WT, the random coil conformation is enhanced with an increase in concentration. This is also true for mutant I23V. For these three variants, WT, I23V, and N58A, there is an increase in random coil content when the concentration is increased, and not just a pure increase in β-sheet content.

Regardless, F65A, the mutant not prone to aggregation (*5*) and rather unstable (*19*), shows, at acidic pH and 20 μM, a spectrum similar to that at neutral pH. With an increase in concentration, the helical content decreases only 5% in favor of the β-sheet. The random coil contribution is similar under all the conditions studied (Table 1). Thus, it is quite possible that mutation of this residue, which interacts with part of the hydrophobic core in the WT, generates a β-conformation with some similarities to that present in the final fibril, which will be more populated at the concentration required for the IR experiments.

DISCUSSION

Assignment of the Aggregation Bands for the Wild-Type Protein. Infrared band assignment is not a straightforward procedure because of the sensitivity of IR to combined structural and environmental factors (*36*). Despite the hallmark β-conformation of amyloid fibrils (*37*), it has been reiteratively shown by IR that the amide I′ peaks cluster between 1630 and 1640 cm^{-1} for β-sheet proteins whereas for ordered (amyloid-like fibrils) or amorphous aggregates they extend from 1611 to 1630 cm^{-1} (*30*). This structural difference makes IR a very suitable technique for following fibril formation processes from all types of protein folds.

Initially, the band at 1619 cm^{-1} represents 14% of the amide component. This indicates that a portion of the protein is initially aggregated. This aggregation, although contributing slightly to the spectra, could not be avoided at the acidic pH of the experiment, especially at the required protein concentration for the IR (5 mg/mL, 544 μM). Nevertheless, the electron micrograph obtained under the same conditions (Figure 4A, time zero) does not show the presence of any structured amyloid fibril but rather some irregular wormlike structures, similar to those seen previously for β_2-microglobulin (*33*). These less structured fibrils presumably are responsible for the initial band at 1619 cm^{-1}, similar to the 1622 cm^{-1} band previously seen for β_2-microglobulin wormlike fibrils (*38*), whereas the final position at 1616 cm^{-1} would

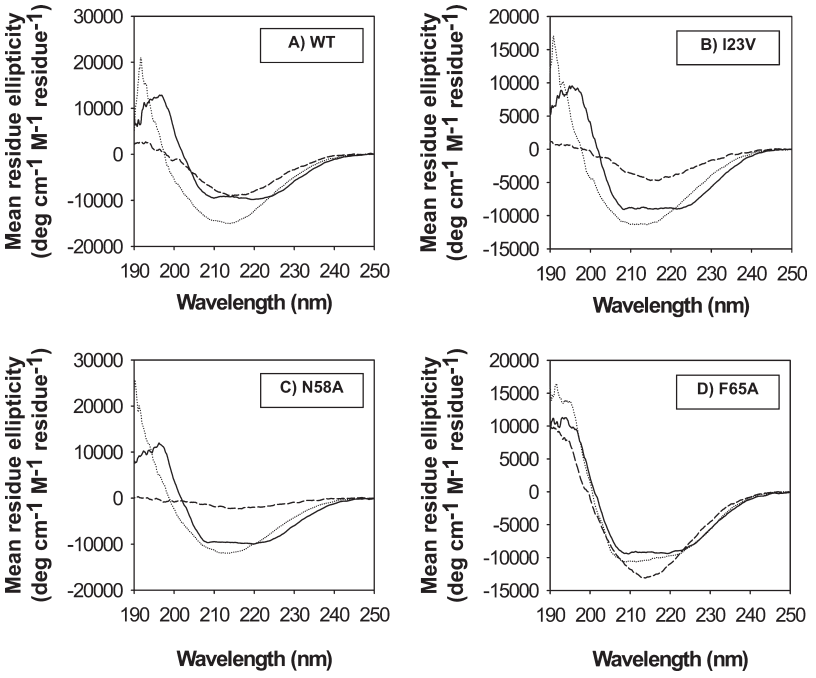

FIGURE 5: Comparison among the native and amyloid-induced conformations of WT ADA2h and the destabilized mutants by circular dichroism. Conformations of WT and mutants I23V, N58A, and F65A analyzed by circular dichroism spectroscopy under native conditions, at pH 7 (solid line), and after induction of amyloidogenesis by temperature, at pH 3, at a protein concentration of 20 μM (dotted line) and at a protein concentration of 200 μM (dashed line). All variants show a similar $\alpha + \beta$ spectrum at pH 7, and an all-β spectrum at pH 3 typical of amyloidogenic aggregation, with the exception of F65A at 20 μM. Under those conditions, this mutant exhibits a nativelike spectrum; however, at 200 μM (similar to the IR conditions), it is able to form these aggregates.

Table 1: Secondary Structure Content of ADA2h under Native and Amyloid-Induced Conditions Followed by Circular Dichroism[a]

	α-helix (%)	β-sheet (%)	β-turn (%)	random (%)
WT at pH 7, 20 μM	32	20	12	36
WT at pH 3, 20 μM	24	29	11	36
WT at pH 3, 200 μM	8	38	11	43
I23V at pH 7, 20 μM	31	20	13	36
I23V at pH 3, 20 μM	17	35	12	36
I23V at pH 3, 200 μM	6	42	12	40
N58A at pH 7, 20 μM	32	20	12	36
N58A at pH 3, 20 μM	9	43	11	37
N58A at pH 3, 200 μM	7	39	12	42
F65A at pH 7, 20 μM	27	25	12	36
F65A at pH 3, 20 μM	27	25	12	36
F65A at pH 3, 200 μM[b]	21	31	11	37

[a]Deconvolution of the circular dichroism spectra of ADA2h variants at 20 μM and neutral pH and at 20 and 200 μM at acidic pH. It should be noted that both the β-sheet and the random coil components experience an increase in percentage when the protein is placed under conditions that favor aggregation (low pH and high protein concentration). It is important to determine that circular dichroism is not able to discern between native and aggregated β-structures. [b]The spectrum of F65A at 200 μM and pH 3 is too noisy in the far-UV region because of detector saturation, making its deconvolution unreliable.

correspond to the more structured amyloid fibrils. This highlights the different nature of these aggregates, as compared to that characteristic of the mature amyloid fibrils, and might represent a ground state from a different aggregation pathway (*33*). It is noteworthy that inclusion bodies and thermally induced nonfibrillar aggregates also present a band located around 1625 cm^{-1} (*33*).

Nucleation and Reorganization. It has recently been reported that the amide I′ band maximum of native β-proteins depends on the average number of strands per sheet, decreasing the wavenumber when the number of strands is increased (*30*). This feature is also suggested by ab initio calculations (*39*). A location at 1615 cm^{-1} was previously reported for WT ADA2h amyloid fibrils that were induced at 90 °C for 30 min (*14*). In this study, designed to follow the process, the temperature was increased from 20 to 90 °C over 10 min and maintained afterward at 90 °C for 30 min, and a final band of 1616 cm^{-1} was reached. Despite this small difference in the position of the band, the samples incubated in the same way as in the IR experiments show by TEM the unequivocal presence of amyloid fibrils.

A reorganization step in the formation of amyloid fibrils of ADA2h can be elucidated by the fact that (i) the β-sheet bands are different in the native and initially aggregated protein, with wavelengths at 1632 and 1619 cm^{-1}, respectively, and (ii) the final fibril shows a prominent band at 1616 cm^{-1}. Also, a reorganization event was described for this domain when the very early kinetics of acquisition of β-structure from the unfolded state by CD induced by pH jump was studied (*5*). There are several proteins in which a conformational reorganization of the nucleus has been reported to achieve ordered fibrillation (*30*, *40*−*42*). However, this is not the case for β_2m, whose native β-sheets are almost identical to aggregated β-sheets (*38*). In addition, there is also a recent computer simulation indicating that hydrophobic residues are sequestered away from the solvent during the nucleation step, whereas during fibril formation oligomers undergo a process of reorganization driven by interchain hydrogen bonding interactions that induce the formation of β-sheet-rich assemblies (*43*).

Influence of Aggregation Propensity and Stability. In a previous work, we determined the concentration-dependent rate constant (k_1, nucleation) and the concentration-independent rate constant (k_2, reorganization) for a large battery of single-residue

variants and demonstrated that it is the interplay between stability and the propensity of a sequence to form ordered aggregates that determines the aggregation outcome for a protein (*5*). In the work presented here, the wild-type protein (k_1 = 0.40 s^{-1}), a slowly aggregating mutant (I23V) (k_1 = 0.14 s^{-1}), a rapidly aggregating mutant (N58A) (k_1 = 0.86 s^{-1}), and a mutant not prone to (F65A) (k_1 = 0.00 s^{-1}) have been chosen to study the process of amyloid fibril formation by IR. The induction by temperature has been performed from the folded state at acidic pD to evaluate the combined contribution of stability and aggregation propensity.

The initial area of the band around 1619 cm^{-1} is greater in all mutants than in the wild-type protein, demonstrating that destabilization of the native state, with respect to the aggregation intermediate ensemble, is coupled with an increased propensity for nonfibrillar aggregation. In the case of mutant N58A, its tendency to form amyloid fibrils is responsible for a greater initial area of this hallmark band.

At time zero, all of the variants, with the exception of I23V, form wormlike structures as seen by TEM. The lack of these structures for I23V at time zero could be related to its ability to form non-native interactions during the transition state of its folding reaction (*19*). The presence of such structures, especially for the most unstable mutant, F65A, reinforces the idea that wormlike structures correspond to a ground state that is easily reached from partially unfolded proteins. This ground state is in direct competition and favored, with respect to amyloid fibril formation, under our initial experimental conditions (*33*). However, thermal denaturation facilitates the formation of amyloid fibrils, presumably by allowing the buried regions within the domains to be exposed, which leads to the nucleation-dependent process of ordered aggregation. This reflects the fact that ADA2h would follow the refolding model among the monomer structural reorganization models proposed by Eisenberg et al. (*8*).

Apart from the results discussed, the 2D-COS maps correlate the bands and shed some light on the dynamics of the process. The synchronous map for the wild type shows that the major interaction is between bands that have been assigned to partially unfolded α-helices and the amyloid fibril. The spectra of the mutants present broadened bands, which could reflect the fact that these variants are not initially as structured as the wild-type protein, in accordance with their lower stability (*19*).

In spite of the differences observed for wild-type ADA2h and its mutants, their aggregation processes all culminate in the formation of amyloid-like fibrils with equivalent characteristics. This indicates that when experimental conditions are forced, i.e., protein concentration, variants with different tendencies to aggregate and stabilities are capable of aggregating as ordered fibrils. Although sequence context is relevant to the kinetics of amyloid fibril formation (*5*), the mechanism by which a protein reaches a thermodynamically stable aggregate should be intrinsic to the polypeptide chain (*1*).

SUPPORTING INFORMATION AVAILABLE

Analysis of the main components of the amide I′ band for ADA2h variants (Table 1), analysis of the minor components of the amide I′ band for ADA2h variants (Table 2), kinetics of the formation of amyloid fibrils by four variants of ADA2h followed by FT-IR (Figure 1), and plot showing variations in the position and area of the main bands in the FT-IR spectra during amyloid formation kinetics (Figure 2). This material is available free of charge via the Internet at http://pubs.acs.org.

REFERENCES

1. Dobson, C. M. (2003) Protein Folding and Misfolding. *Nature 426*, 884–890.
2. Jahn, T. R., and Radford, S. E. (2005) The Yin and Yang of Protein Folding. *FEBS J. 272*, 5962–5970.
3. Chiti, F., Taddei, N., Baroni, F., Capanni, C., Stefani, M., Ramponi, G., and Dobson, C. M. (2002) Kinetic Partitioning of Protein Folding and Aggregation. *Nat. Struct. Biol. 9*, 137–143.
4. Chiti, F., Stefani, M., Taddei, N., Ramponi, G., and Dobson, C. M. (2003) Rationalization of the Effects of Mutations on Peptide and Protein Aggregation Rates. *Nature 424*, 805–808.
5. Cerda-Costa, N., Esteras-Chopo, A., Aviles, F. X., Serrano, L., and Villegas, V. (2007) Early Kinetics of Amyloid Fibril Formation Reveals Conformational Reorganisation of Initial Aggregates. *J. Mol. Biol. 366*, 1351–1363.
6. Fernandez-Escamilla, A. M., Rousseau, F., Schymkowitz, J., and Serrano, L. (2004) Prediction of Sequence-Dependent and Mutational Effects on the Aggregation of Peptides and Proteins. *Nat. Biotechnol. 22*, 1302–1306.
7. Pawar, A. P., Dubay, K. F., Zurdo, J., Chiti, F., Vendruscolo, M., and Dobson, C. M. (2005) Prediction of "Aggregation-Prone" and "Aggregation-Susceptible" Regions in Proteins Associated with Neurodegenerative Diseases. *J. Mol. Biol. 350*, 379–392.
8. Nelson, R., and Eisenberg, D. (2006) Recent Atomic Models of Amyloid Fibril Structure. *Curr. Opin. Struct. Biol. 16*, 260–265.
9. Harrington, P. B., Urbas, A., and Tandler, P. J. (2000) Two-Dimensional Correlation Analysis. *Chemom. Intell. Lab. Syst. 50*, 149–174.
10. Noda, I. (2007) Two-Dimensional Correlation Analysis Useful for Spectroscopy, Chromatography, and Other Analytical Measurements. *Anal. Sci. 23*, 139–146.
11. Iloro, I., Chehin, R., Goni, F. M., Pajares, M. A., and Arrondo, J. L. (2004) Methionine Adenosyltransferase α-Helix Structure Unfolds at Lower Temperatures than β-Sheet: A 2D-IR Study. *Biophys. J. 86*, 3951–3958.
12. Iloro, I., Goni, F. M., and Arrondo, J. L. (2005) A 2D-IR Study of Heat- and [^{13}C]Urea-Induced Denaturation of Sarcoplasmic Reticulum Ca^{2+}-ATPase. *Acta Biochim. Pol. 52*, 477–483.
13. Pastrana-Rios, B. (2001) Mechanism of Unfolding of a Model Helical Peptide. *Biochemistry 40*, 9074–9081.
14. Villegas, V., Zurdo, J., Filimonov, V. V., Aviles, F. X., Dobson, C. M., and Serrano, L. (2000) Protein Engineering as a Strategy to Avoid Formation of Amyloid Fibrils. *Protein Sci. 9*, 1700–1708.
15. Villanueva, J., Villegas, V., Querol, E., Aviles, F. X., and Serrano, L. (2003) Monitoring Disappearance of Monomers and Generation of Resistance to Proteolysis during the Formation of the Activation Domain of Human Procarboxypeptidase A2 (ADA2h) Amyloid Fibrils by Matrix-Assisted Laser-Desorption Ionization-Time-of-Flight-MS. *Biochem. J. 374*, 489–495.
16. Villegas, V., Azuaga, A., Catasus, L., Reverter, D., Mateo, P. L., Aviles, F. X., and Serrano, L. (1995) Evidence for a Two-State Transition in the Folding Process of the Activation Domain of Human Procarboxypeptidase A2. *Biochemistry 34*, 15105–15110.
17. Villegas, V., Viguera, A. R., Aviles, F. X., and Serrano, L. (1996) Stabilization of Proteins by Rational Design of α-Helix Stability Using Helix/Coil Transition Theory. *Folding Des. 1*, 29–34.
18. Viguera, A. R., Villegas, V., Aviles, F. X., and Serrano, L. (1997) Favourable Native-Like Helical Local Interactions can Accelerate Protein Folding. *Folding Des. 2*, 23–33.
19. Villegas, V., Martinez, J. C., Aviles, F. X., and Serrano, L. (1998) Structure of the Transition State in the Folding Process of Human Procarboxypeptidase A2 Activation Domain. *J. Mol. Biol. 283*, 1027–1036.
20. Fernandez, A. M., Villegas, V., Martinez, J. C., Van Nuland, N. A., Conejero-Lara, F., Aviles, F. X., Serrano, L., Filimonov, V. V., and Mateo, P. L. (2000) Thermodynamic Analysis of Helix-Engineered Forms of the Activation Domain of Human Procarboxypeptidase A2. *Eur. J. Biochem. 267*, 5891–5899.
21. Villanueva, J., Canals, F., Villegas, V., Querol, E., and Aviles, F. X. (2000) Hydrogen Exchange Monitored by MALDI-TOF Mass Spectrometry for Rapid Characterization of the Stability and Conformation of Proteins. *FEBS Lett. 472*, 27–33.
22. Villanueva, J., Villegas, V., Querol, E., Aviles, F. X., and Serrano, L. (2002) Protein Secondary Structure and Stability Determined by Combining Exoproteolysis and Matrix-Assisted Laser desorption/ionization Time-of-Flight Mass Spectrometry. *J. Mass Spectrom. 37*, 974–984.
23. Arrondo, J. L., and Goni, F. M. (1999) Structure and Dynamics of Membrane Proteins as Studied by Infrared Spectroscopy. *Prog. Biophys. Mol. Biol. 72*, 367–405.

24. Arrondo, J. L. R., Iloro, I., Aguirre, J., and Goni, F. M. (2004) A Two-Dimensional IR Spectroscopic (2D-IR) Simulation of Protein Conformational Changes. *Spectroscopy 18*, 49–58.
25. Lopez De La Paz, M., Goldie, K., Zurdo, J., Lacroix, E., Dobson, C. M., Hoenger, A., and Serrano, L. (2002) De Novo Designed Peptide-Based Amyloid Fibrils. *Proc. Natl. Acad. Sci. U.S.A. 99*, 16052–16057.
26. Whitmore, L., and Wallace, B. A. (2004) DICHROWEB, an Online Server for Protein Secondary Structure Analyses from Circular Dichroism Spectroscopic Data. *Nucleic Acids Res. 32*, W668–W673.
27. Lobley, A., Whitmore, L., and Wallace, B. A. (2002) DICHROWEB: An Interactive Website for the Analysis of Protein Secondary Structure from Circular Dichroism Spectra. *Bioinformatics 18*, 211–212.
28. Lees, J. G., Miles, A. J., Wien, F., and Wallace, B. A. (2006) A Reference Database for Circular Dichroism Spectroscopy Covering Fold and Secondary Structure Space. *Bioinformatics 22*, 1955–1962.
29. Bouchard, M., Zurdo, J., Nettleton, E. J., Dobson, C. M., and Robinson, C. V. (2000) Formation of Insulin Amyloid Fibrils Followed by FTIR Simultaneously with CD and Electron Microscopy. *Protein Sci. 9*, 1960–1967.
30. Zandomeneghi, G., Krebs, M. R., McCammon, M. G., and Fandrich, M. (2004) FTIR Reveals Structural Differences between Native β-Sheet Proteins and Amyloid Fibrils. *Protein Sci. 13*, 3314–3321.
31. Reverter, D., Ventura, S., Villegas, V., Vendrell, J., and Aviles, F. X. (1998) Overexpression of Human Procarboxypeptidase A2 in *Pichia pastoris* and Detailed Characterization of its Activation Pathway. *J. Biol. Chem. 273*, 3535–3541.
32. Jimenez, M. A., Villegas, V., Santoro, J., Serrano, L., Vendrell, J., Aviles, F. X., and Rico, M. (2003) NMR Solution Structure of the Activation Domain of Human Procarboxypeptidase A2. *Protein Sci. 12*, 296–305.
33. Gosal, W. S., Morten, I. J., Hewitt, E. W., Smith, D. A., Thomson, N. H., and Radford, S. E. (2005) Competing Pathways Determine Fibril Morphology in the Self-Assembly of β2-Microglobulin into Amyloid. *J. Mol. Biol. 351*, 850–864.
34. Harper, J. D., and Lansbury, P. T., Jr. (1997) Models of Amyloid Seeding in Alzheimer's Disease and Scrapie: Mechanistic Truths and Physiological Consequences of the Time-Dependent Solubility of Amyloid Proteins. *Annu. Rev. Biochem. 66*, 385–407.
35. Smith, D. P., Giles, K., Bateman, R. H., Radford, S. E., and Ashcroft, A. E. (2007) Monitoring Copopulated Conformational States during Protein Folding Events using Electrospray Ionization-Ion Mobility Spectrometry-Mass Spectrometry. *J. Am. Soc. Mass Spectrom. 18*, 2180–2190.
36. Arrondo, J. L., Echabe, I., Iloro, I., Hernando, M. A., de la Cruz, F., and Goni, F. M. (2003) A Bacterial TrwC Relaxase Domain Contains a Thermally Stable α-Helical Core. *J. Bacteriol. 185*, 4226–4232.
37. Serpell, L. C., Fraser, P. E., and Sunde, M. (1999) X-Ray Fiber Diffraction of Amyloid Fibrils. *Methods Enzymol. 309*, 526–536.
38. Jahn, T. R., Tennent, G. A., and Radford, S. E. (2008) A Common β-Sheet Architecture Underlies in Vitro and in Vivo β2-Microglobulin Amyloid Fibrils. *J. Biol. Chem. 283*, 17279–17286.
39. Kubelka, J., and Keiderling, T. A. (2001) The Anomalous Infrared Amide I Intensity Distribution in ^{13}C Isotopically Labeled Peptide β-Sheets Comes from Extended, Multiple-Stranded Structures: An Ab Initio Study. *J. Am. Chem. Soc. 123*, 6142–6150.
40. Cordeiro, Y., Kraineva, J., Suarez, M. C., Tempesta, A. G., Kelly, J. W., Silva, J. L., Winter, R., and Foguel, D. (2006) Fourier Transform Infrared Spectroscopy Provides a Fingerprint for the Tetramer and for the Aggregates of Transthyretin. *Biophys. J. 91*, 957–967.
41. Serio, T. R., Cashikar, A. G., Kowal, A. S., Sawicki, G. J., Moslehi, J. J., Serpell, L., Arnsdorf, M. F., and Lindquist, S. L. (2000) Nucleated Conformational Conversion and the Replication of Conformational Information by a Prion Determinant. *Science 289*, 1317–1321.
42. Plakoutsi, G., Bemporad, F., Calamai, M., Taddei, N., Dobson, C. M., and Chiti, F. (2005) Evidence for a Mechanism of Amyloid Formation Involving Molecular Reorganisation within Native-Like Precursor Aggregates. *J. Mol. Biol. 351*, 910–922.
43. Cheon, M., Chang, I., Mohanty, S., Luheshi, L. M., Dobson, C. M., Vendruscolo, M., and Favrin, G. (2007) Structural Reorganisation and Potential Toxicity of Oligomeric Species Formed during the Assembly of Amyloid Fibrils. *PLoS Comput. Biol. 3*, 1727–1738.